Electronic Supplementary Material (ESI) for Nanoscale.
This journal is © The Royal Society of Chemistry 2024

Electronic Supplementary Information:

Discarding metal incorporation in pyrazole macrocycles and the role of the substrate on single-layer the assemblies.

J. Lobo-Checa, S. J. Rodríguez, L. Hernández-López, L. Herrer,
Mario C. G. Passeggi (Jr.), P. Cea, and J. L. Serrano

This supplementary material contains the following sections:

- S1. The Materials and Methods section.
- S2. The supplementary table reporting the supercell parameters obtained from the DFT calculations
- S3. Supplementary figures with self-explanatory captions.
- S4. Bond length comparison between different arrangements.
- S5. Supplementary references.

S1. MATERIALS AND METHODS

PBP chemical synthesis and sample preparation

The synthesis of the 1,4-bis - ((1H-pyrazol-4-yl)ethynyl) has been previously described.[1-2] PBP was evaporated in UHV at a temperature of 105°C from a homemade Knudsen cell onto the substrates held at RT. The deposition rate was monitored by a homemade quartz resonator at the exit of the Knudsen cell at a rate of ~0.03 monolayers per minute. The Cu(111), Ag(111) and Au(111) crystals were cleaned by repeated cycles of ionized argon sputtering ($9\cdot10^{-6}$ mbar, 1 keV, 10 mA, 20 minutes) and annealing (to 500°C, 400°C and 530°C) for 10 minutes.

STM experimental details.

Scanning tunneling microscopy experiments were generally performed in constant current mode (unless indicated otherwise) using an ultra-high vacuum low-temperature scanning tunneling microscope (Omicron LT-STM) operating under 5 K and with chamber pressures well below $1\cdot10^{-10}$ mbar. A tungsten tip was used in all cases and the voltages are referred to the sample (grounded tip).

The CO functionalization of the tip was achieved by attaching a CO molecule at the tip apex after adsorbing CO molecules on the surface (P_{CO} = $1\cdot10^{-8}$ mbar, 2.5 minutes, T_S = 5-10 K). Bond-resolved images required scanning in constant-height mode at -0.16 mV (STM bias offset). Note that we use raw data (without Laplacian filters) in the figures displayed for this mode.

Computational details

First-principles calculations based on Density Functional Theory (DFT) were performed using the norm-conservative pseudopotentials and pseudo-atomic orbitals (PAOs) as implemented in the OpenMX3.9 code.[3,4] The electronic exchange–correlation effects were treated within the generalized gradient approximation (GGA) as the functional proposed by Perdew, Burke, and Ernzerhof (PBE).[5] Furthermore, we used the DFT-D3 approach for the correction of van der

Waals interactions.[6] Basis functions were created using a confinement scheme and labeled as C6.0-s3p2d2, N6.0-s3p2d2, H7.0-s2p2d1, where C, N, and H denote the chemical elements, the following numbers were the cut-off radius (Bohr radius), and the last set of symbols after the dash represent the primitive orbitals, e.g., s2 indicates the use of two orbitals for s component. A cut-off energy of 180 Ry in the numerical integration and the solution of the Poisson equation, and a **k**-point mesh of 5 x 5 x 1 was used for the self-consistency.

To understand the self-assembly process of PBP, we first modeled two gas-phase systems: (i) hexagonal arrangement (Hex-PBP) and (ii) oblique arrangement (Ob-PBP), each with 90 and 118 atoms per unit cell, respectively. The supercell of Hex-PBP system contains three PBP molecules, which are in their pristine configuration. On the other hand, the supercell of Ob-PBP system has a total of four PBP molecules, such that two molecules are in their pristine configuration and two are deprotonated on the pyrazole ring. From the calculated STM images we find a more stable and regular assembly of the deprotonated arrangement compared to the pristine monomer lattice. Importantly, we find in the former arrangement an alternating rotation in the pyrazole rings that is absent on the latter. These pyrazole rotations are fully aligned with the experimental images obtained by STM that, in a first approximation, supports the validity of the model presented in the main text.

All atoms were allowed to move freely during the optimization procedure (atomic positions were converged to below 0.02 eV/Å). For the most stable configurations the corresponding STM images were calculated using the Tersoff-Hamman approach,[7] which considers that the local density of states (LDOS) contributing to the current lies in the energy window $[E_F\text{-}e\cdot V_{bias}, E_F]$, where E_F, e and V_{bias} are the Fermi energy, the electron charge and the bias voltage, respectively. Data analysis and processing were made by using the WSxM free software.[8]

S2. SUPPLEMENTARY TABLE

System	Supercell parameters	Number of atoms	$d_{N\cdots H\text{-}N}$ (nm)	$d_{N\cdots H\text{-}C}$ (nm)	$d_{C\text{-}H\cdots H\text{-}N}$ (nm)	θ (°)
Hexagonal arrangement	a = 3.37 nm b = 3.37 nm c = 3.00 nm α_{a-b} =60°	90	0.188	-	-	-
Oblique arrangement	a = 2.315 nm b = 3.608 nm c = 3.000 nm α_{a-b} = 103.89°	118	0.187	0.240	0.267	36.5°

Table 1. Supercell parameters after the relaxation processes of the hexagonal and oblique arrangements obtained in the gas-phase by DFT. The unit cells obtained are defined by the lengths **a** and **b** and the angle $\alpha_{a\text{-}b}$, which are represented in Figs 3d and 5c of the main text. The parameter **c** indicates the interplane separation, which is required for the calculations and is chosen to avoid vertical interactions between layers. Number of atoms, $d_{N\cdots H\text{-}N}$, $d_{N\cdots H\text{-}C}$, $d_{C\text{-}H\cdots H\text{-}N}$ and θ are the number of the atoms per supercell in each system, the average distance of the hydrogen bond between N⋯H-N, the average distance of the alternative hydrogen bond between N⋯H-C, the average distance between repulsive hydrogens and the average rotation angle of the modified pyrazole ring, respectively. See Fig. 5 and main text for details.

S3. SUPPLEMENTARY FIGURES

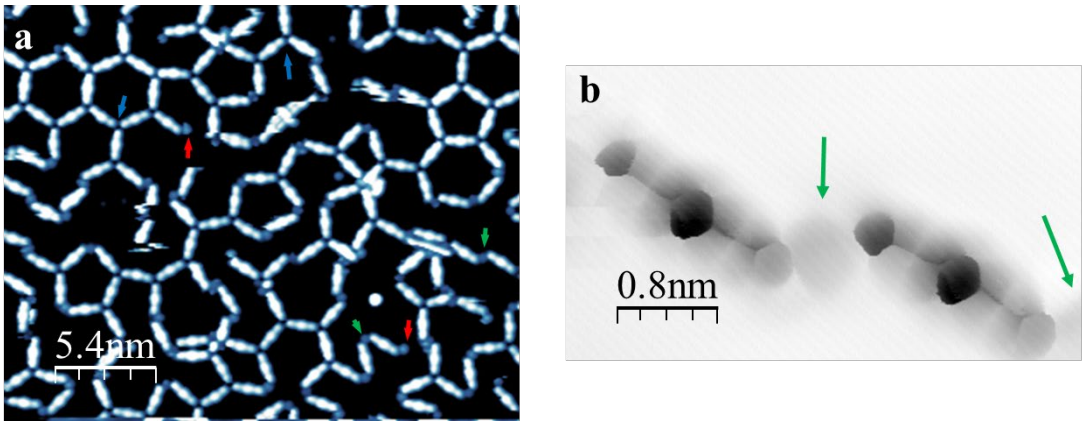

Figure S1. High-resolution STM images of PBP on Au(111) of non-hexagonal regions acquired with a CO funcionalized tip. (a) Note that Au adatoms are extensively observed as dim blue spheres (cf. red and green arrows) except at regular three-fold coordination (4dim blue arrows) featuring double H-bonds. (b) Bond-resolved imaging obtained at constant height mode with a CO functionalized tip showing the Au adatoms as faint shadows (green arrows). Note that the pyrazole rings in contact with the Au appear at different heights, judging by their different contrast and in comparison with the common intensity of their central rings.
STM image details: (a) Constant current mode, 27.0×21.5 nm^2, 0.01 V, 30 pA; (b) Constant height mode image, 3.8×2.1 nm^2, -0.16 mV (STM bias offset).

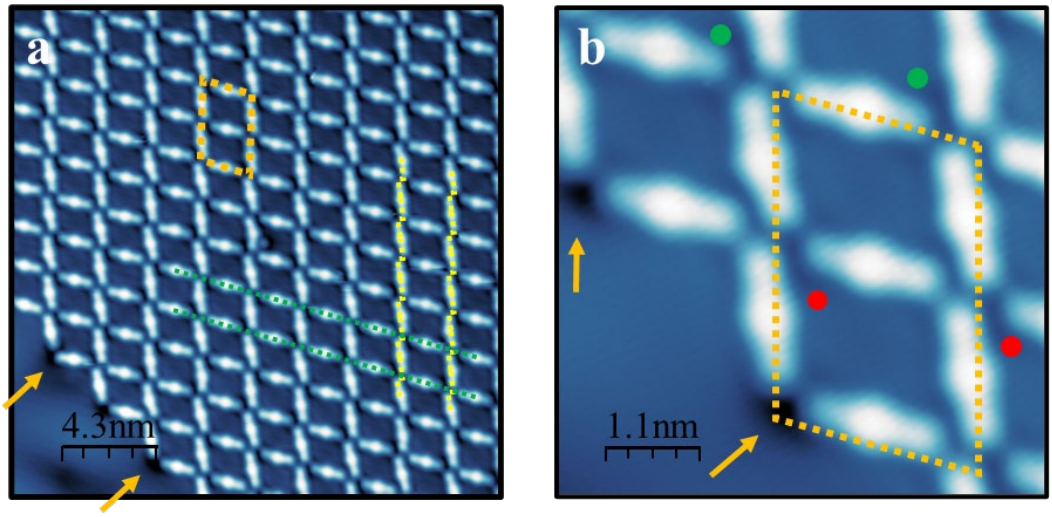

Figure S2. STM images of the high-temperature (above 85 ºC) arrangement of PBP on Ag(111) featuring an island border. (a) High-resolution overview of the oblique arrangement. (b) Close up of the oblique network at the island termination. The unit cell of is shown in orange parallel to the discontinuous yellow and green lines of (a). The dark intensity areas at the uncoordinated positions (marked by orange arrows) agrees with a charge depletion case originating from the formation of a bond between the rotated pyrazoles and the Ag substrate.
STM image details: (a) 21.5×21.5 nm^2, 0.01 V, 130 pA; (b) 5.4×5.4 nm^2, 0.01 V, 130 pA.

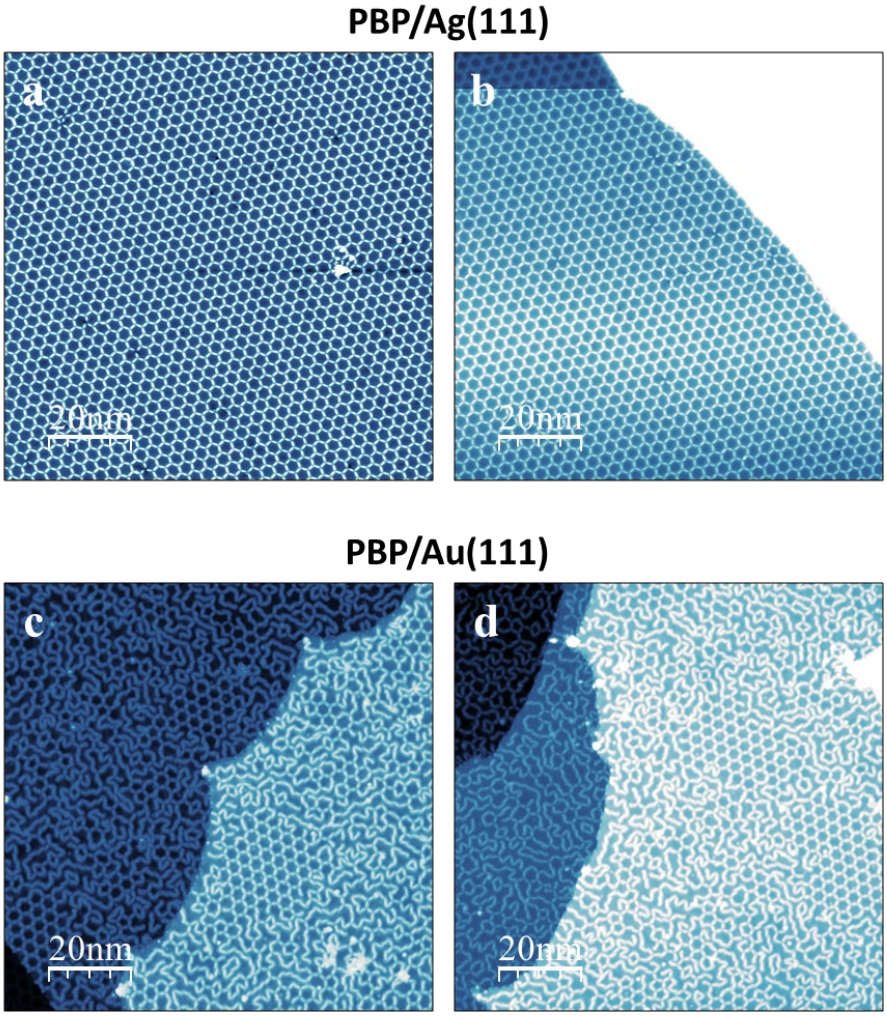

Figure S3. STM images of PBP on Ag(111) and Au(111) after annealing to 75 ºC. In the case of Ag(111) (panels (a) and (b)) the hexagonal order dramatically improves after such mild annealing of the system. Contrarily, in the case of Au(111) (panels (c) and (d)) the porous structure is replaced by the chain-like structure when using the same annealing conditions due to the increased density of metal adatoms at the surface during annealing.
STM image details: (a) and (b) 100×100 nm^2, -0.10 V, 130 pA; (c) and (d) 100×100 nm^2, -1.0 V, 130 pA.

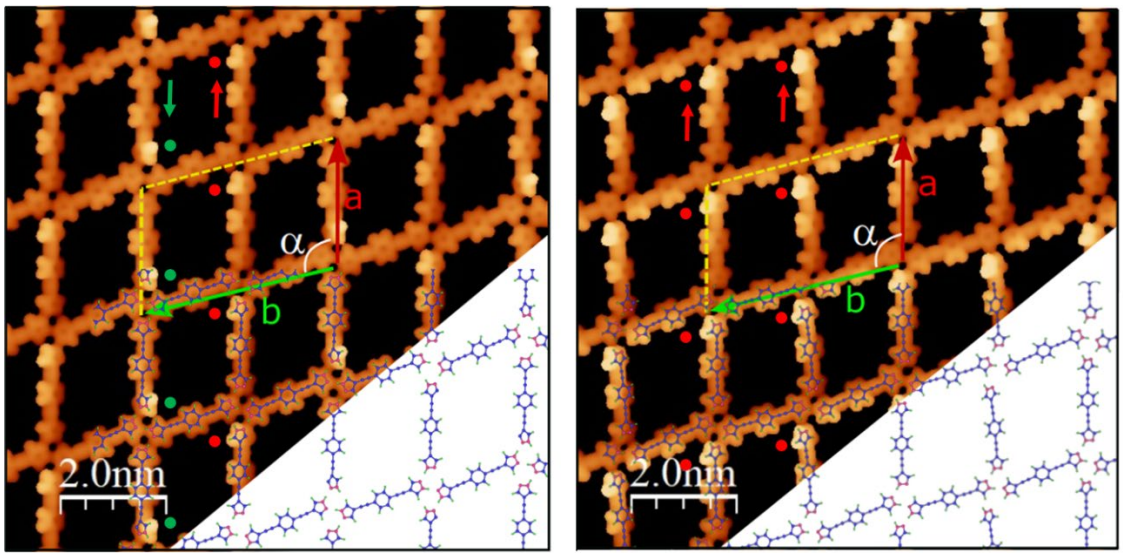

Figure S4. Simulated STM images of deprotonated (left) and un-deprotonated (right) Oblique arrangements calculated in the gas-phase by DFT. In the deprotonated oblique arrangement, a hydrogen atom from a C-H bond of one pyrazole ring is removed. The non-deprotonated oblique arrangement comprises PBP molecules in their pristine state. The yellow dashed lines correspond to the modeled supercells. In the un-deprotonated case, we find that the molecular arrangement is more irregular and the pyrazole group rotation is always in the same direction, which disagrees with the experimental datasets. The images were simulated with a bias voltage of V_b = 1 V and have a lateral size of 10×10 nm^2.

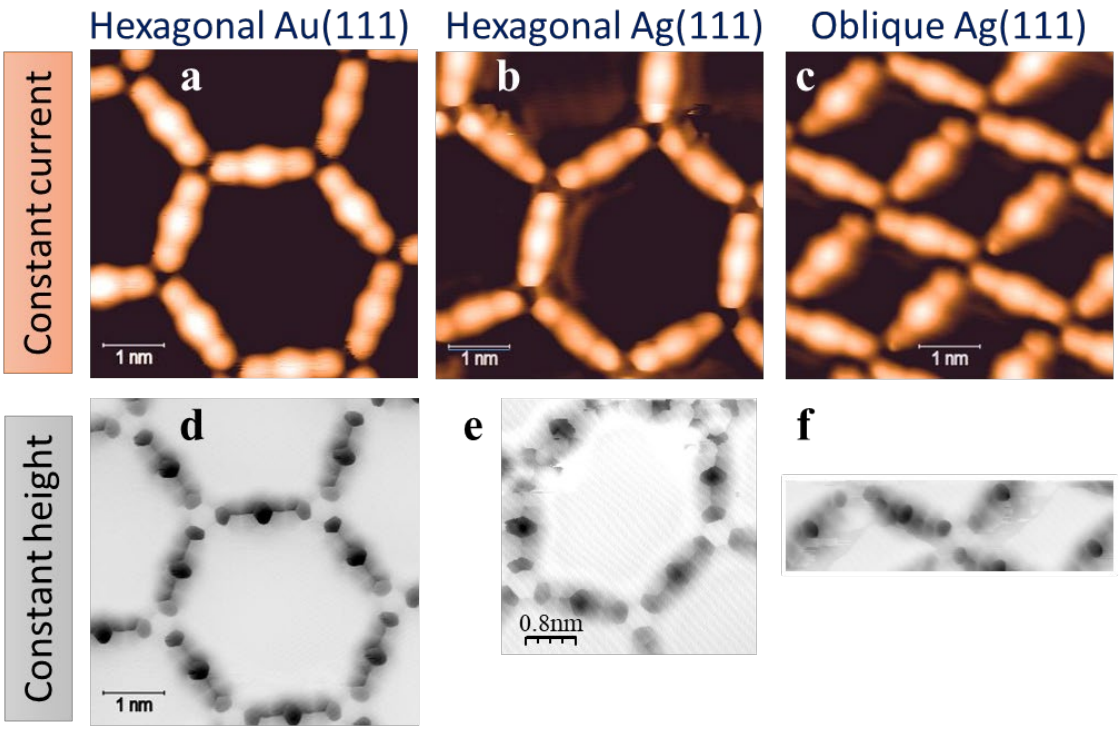

Figure S5. Comparison between (a,d) hexagonal on Au(111), (b,e) hexagonal on Ag(111) and (c,f) oblique on Ag(111) arrangements on scaled images with the same aspect ratio. In the top row constant current images are shown and in the bottom row bond-resolved images obtained at constant height with a CO functionalized tip. Each row has been acquired with similar scanning parameters to help for a direct visual comparison. Within the experimental error we find in average that the N-H···N bond distances are practically identical in all arrangements, discarding metal incorporation in the coordination. STM acquisition details: (a) 10 mV, 30 pA, (b) 10 mV, 30 pA; (c) 10 mV, 50 pA; (d) to (f) constant height images at -0.16 mV (STM bias offset).

S4. BOND LENGTH COMPARISON BETWEEN DIFFERENT ARRANGEMENTS.

Fig. S5 shows scaled STM images witht the same aspect ratio acquired at constant current in the top row and at constant height (bond-resolved) in the bottom row of the two structures formed on both Au(111) and Ag(111). As the images on each row are acquired with similar experimental conditions, we can directly compare them by rows. This avoids errors when comparing datasets measured with different experimental conditions and image sizes. For instance, in bond-resolved images (bottom row in Fig. S5), there is a limited contribution from the molecular electronic cloud compared to the constant current images (top row in Fig. S5).

From a visual inspection, we find in the hexagonal network of Ag(111) a certain flexibility in the hydrogen bond-length, but in average (within the experimental error) the N-H···N bond distances are practically identical in the all arrangements. Importantly, in the hexagonal structures we can discard the metal adatom coordination based on the structural coincidence on the three substrates because the elements exhibit very different electronic affinities and atomic radii. The fact that we observe that the N-H···N bond distance in the oblique arrangement is practically identical to the hexagonal network (as shown in Fig. S5) is

incompatible with any metal incorporation. Moreover, the agreement with the STM simulated images is additional proof that Ag adatoms can be safely excluded from this oblique structure.

S5. SUPPLEMENTARY REFERENCES

1.- S. Galli, A. Maspero, C. Giacobbe, G. Palmisano, L. Nardo, A. Comotti, I. Bassanetti, C.P. Sozzanic and N. Masciocchia. When long bis(pyrazolates) meet late transition metals: structure, stability and adsorption of metal–organic frameworks featuring large parallel channels. J. Mater. Chem. A, 2014, 2, 12208–12221.

2.- I.L. Herrer, A.K. Ismael, D.C. Milán, A. Vezzoli, S. Martín, A. González-Orive, I. Grace, C. Lambert, J.L. Serrano, R.J. Nichols, P. Cea. Unconventional single molecule conductance behavior for a new heterocyclic anchoring group: pyrazolyl. J. Phys. Chem. Lett. 2018, 9, 5364−5372.

3. T. Ozaki. Variationally optimized atomic orbitals for large-scale electronic structures. Phys. Rev. B 2003, 67, 15510.

4. T. Ozaki, H. Kino. Numerical atomic basis orbitals from H to Kr. Phys. Rev. B 2004, 69, 195113.

5. J.P. Perdew, K. Burke, M. Ernzerhof. Generalized gradient approximation made simple. Phys. Rev. Lett. 1997, 78, 3865.

6. S. Grimme, S. Ehrlich, L. Goerigk. Effect of the damping function in dispersion corrected density functional theory. J. Comput. Chem. 2011, 32, 1456.

7. J. Tersoff, D.R. Haman. Theory of the scanning tunneling microscope. Phys. Rev. B. 1985, 31, 805.

8. I. Horcas, R. Fernández, J.M. Gómez-Rodríguez, J. Colchero, J. Gómez-Herrero, A.M. Baró. WS×M: A software for scanning probe microscopy and a tool for nanotechnology. Rev Sci Instrum. 2007, 78, 013705.